Fabrication and Absorption Intensity Analyses of Er_2O_3 Nanoparticles Suspended in Polymethyl Methacrylate

Sreerenjini Chandra,[1] John B. Gruber,[1] Gary W. Burdick,[2] Dhiraj K. Sardar[1]

[1]*Department of Physics and Astronomy, The University of Texas at San Antonio, San Antonio, Texas 78249–0697*
[2]*Department of Physics, Andrews University, Berrien Springs, Michigan 49104–0380*

Received 28 June 2010; accepted 27 December 2010
DOI 10.1002/app.34058
Published online 21 April 2011 in Wiley Online Library (wileyonlinelibrary.com).

ABSTRACT: Nanoparticles suspended in polymeric host materials are found to have tremendous potential for various photonic and biological applications due to their unique material properties. Polymethyl methacrylate (PMMA) is known to be one of the best vinyl polymers owing to its excellent dimensional quality, weather resistance, easiness of synthesis, resistance to laser damage, and high mechanical strength. In this article, we describe a methodology to fabricate thin discs of nanocrystalline erbium oxide (Er_2O_3) suspended in PMMA (Er_2O_3/PMMA). The optical transparency of PMMA was confirmed in the ultraviolet, visible, and the near-infrared regions of the electromagnetic spectrum, making it possible to observe only the Er_2O_3 spectra over the wavelength investigated. The room-temperature absorption spectrum of Er_2O_3/PMMA has been taken in the 400 to 820 nm wavelength region. Analysis of the spectrum reveals a consistent agreement between our experimental data and those reported earlier for Er^{3+} in nanocrystalline $Er^{3+} : Y_2O_3$. A solid solution exists between Er_2O_3 and $Er^{3+} : Y_2O_3$ in terms of their physical properties. Therefore, our experimental results conclude that the presence of PMMA does not significantly alter the crystal symmetry as well as the co-ordination environment of the Er^{3+} ions in Er_2O_3. Our results also emphasize that the Er_2O_3/PMMA may have future possibilities for numerous technological applications. © 2011 Wiley Periodicals, Inc. J Appl Polym Sci 122: 289–295, 2011

Key words: synthesis; nanoparticles; PMMA; nanocomposites; rare-earth

INTRODUCTION

Polymeric host materials have drawn significant attention in recent years due to their major technological applications such as polymer optical fiber amplifiers, integrated waveguides, and fluorescence and laser systems.[1–5] Studies have proven that polymers can be easily deposited on any kind of substrates commonly used for telecommunication purposes.[6] Additionally, polymer host materials are found to have multifunctional characters such as nonlinear optical and laser responses, making them useful as optical switches, modulators, multiplexers, and frequency converters.[6–8] It has been found that nanoparticles suspended in polymeric hosts (polymer nanocomposites) are slated for applications in fuel cells due to their exceptional qualities of improved conductivity, toughness, and permeability.[9] Studies have shown that there is a limitation of lack of water-resistant capacity when these nanoparticles are doped into several of the nonpolymeric host materials.[10] It is possible to offset this deficiency by suspending them in polymeric compounds.[11] The major advantage of polymer nanocomposites is their ability to be drawn into flexible optical fibers thereby making them potential candidates for various photonic applications such as light emitting diodes and organic based lasers.[5,12,13]

Nanoparticles that are doped with trivalent rare-earth (RE^{3+}) ions possess several unique spectroscopic properties such as sharp absorption and fluorescence, determined by the gradual filling of their 4*f* shells and the ionic radii.[14] Moreover, the RE^{3+} doped materials are found to have excellent photoresistance and long-lasting fluorescence properties.[15] Latest studies have reported that RE^{3+}-doped nanophosphors emit energy in the visible wavelength range through upconversion mechanisms.[16–19] Among the entire group of RE^{3+} ions, trivalent erbium (Er^{3+}) ions have been extensively studied and applied in the technologies of large-scale communication systems such as fiber amplifiers and infra-red lasers where they serve as the active centers for emission of photons and the amplification of IR radiation.[20] Moreover, Er^{3+} ions doped into cubic yttrium oxide ($Er^{3+} : Y_2O_3$), are found to have tremendous applications as high optical and thermal quality laser materials.[10,15,21–26] With the aid of newer technologies, the more expensive single

Correspondence to: D. K. Sardar (dhiraj.sardar@utsa.edu).
Contract grant sponsor: National Science Foundation; contract grant number: DMR-0934218.

crystal form of Er^{3+} : Y_2O_3 is being replaced by its ceramic and thin film counterparts, thereby reducing the material costs and possessing unique physical characteristics more appropriate for current device applications.[25,27–31] Detailed studies have been performed on the mechanical, thermal, and optical properties of these newer materials either in their pure form or as polymer composites.[6,32–35]

Recently, the authors have reported the synthesis and optical characterization of Nd^{3+} : Y_2O_3 nanocrystals doped into a polymer named polymethyl methacrylate (PMMA).[36] PMMA is known to be one of the best vinyl polymers for its unique material properties such as excellent dimensional quality, good weather resistance, simple synthesis technique, resistance to laser damage, and high mechanical strength.[5,12,37,38] Studies have reported the occurrence of amplified-spontaneous emission in Nd^{3+} doped PMMA.[39] Sun et al.[40] have shown that $Eu(DBM)_3Phen$ doped PMMA can be used to develop the laser and amplifier of polymer waveguide. It has also been shown that the laser gain coefficient of Er^{3+} : Y_2O_3 nanoparticles codoped with trivalent cerium (Ce^{3+}) and ytterbium (Yb^{3+}) ions, increases when suspended in the PMMA polymer matrix.[6] There has been reported the occurrence of efficient energy-transfer phenomena from Er^{3+} to other RE^{3+} ions such as holmium (Ho^{3+}), dysprosium (Dy^{3+}), and thulium (Tm^{3+}).[41–43] It is also important to note that Er_2O_3 is of noticeable interest as a host crystal in which the excitation of Er^{3+} ions may be transferred to other RE dopants.[24] Hoskins et al. have proved the efficiency of Ho^{3+} : Er_2O_3 as a unique laser host material which itself provides the pumping mechanism by means of energy transfer.[44]

In this article, we present the fabrication of thin discs of a potential luminescent polymer PMMA suspended with nanocrystalline Er_2O_3, abbreviated as Er_2O_3/PMMA, and the spectroscopic characterization of the Er^{3+} manifolds in it. A detailed study has been performed on the room-temperature absorption spectra of all the Stark energy levels between 12,280 and 22,610 cm^{-1} of Er^{3+} ion in C_2 sites of Er_2O_3 in PMMA. The spectral energy values are compared with the previously obtained experimental energy (Stark) levels for the nanocrystalline Er^{3+} : Y_2O_3[35] covering the same wavelength range.

EXPERIMENTAL

Synthesis and morphology

The Er_2O_3 nanoparticles of approximately 25 nm in diameter were prepared through a hydrothermal precipitation method. The detailed methodology of synthesis has been reported in our previous article.[31] Monomers of methyl methacrylate [MMA, VWR-TCM0087, 99.8%, inhibited with 300 ppm of monomethyl ether of hydroquinone (MEHQ)] were passed through a commercially available (Sigma-Aldrich) inhibitor column to remove the inhibitor. Approximately, 3 mL of the resulting uninhibited MMA solution was poured into a glass vial, to which we added 2, 2′-azobisisobutyronitrile (AIBN) as the initiator in a molar ratio 1 : 1000 with respect to the MMA solution to begin the polymerization. After stirring well, Er_2O_3 nanoparticles were added in a molar ratio 1 : 5 with respect to the entire solution. The final solution was stirred well with continued vigorous stirring at 100°C. The polymerization process begins approximately in an hour. The solution is heated for an additional 3 hours at the same temperature and then allowed to cool overnight. The solid Er_2O_3/PMMA sample is cut and polished into thin discs having an approximate diameter of 1 cm and a thickness of 2 mm. In the same way, a reference sample of pure PMMA was made with AIBN as initiator in the 1 : 1000*M* ratio for a comparison study of the absorption spectra of Er_2O_3/PMMA. The temperature was regulated to the required fixed values by conducting the stirring and heating steps inside a water-bath system which was kept at 100°C.

We used a scanning electron microscope (Hitachi *S*-5500 SEM), a transmission electron microscope (JEOL 1230 TEM), and a high resolution transmission electron microscope (JEOL JEM-2010F TEM) to reveal the appropriate size, shape and distribution of the nanoparticles. The individual nanoparticles are found to be three-dimensional cubic-shaped structures with an average diameter of 25 nm. Figure 1 shows the SEM and TEM images of the Er_2O_3 nanoparticles. X-ray powder diffraction (XRD) analyses of the similar samples[35,45] have verified the cubic bixbyite structure of the Y_2O_3 and therefore that of Er_2O_3 samples. Studies show that the crystal structure is same for both the Er_2O_3 and Y_2O_3 and a solid solution exists between their physical properties.[46,47] The detailed morphology has been depicted in one of our recent publications[6] which includes various microscopic images and size distribution histogram of the Er^{3+} : Y_2O_3 nanoparticles synthesized using the same methodology and containing 0.3 atm % of Er^{3+} ions. The HRTEM images revealed the presence of three distinct sets of lattice planes, with interplanar lattice spacings of 3.06, 2.62, and 1.83 Å representing the *d*222, *d*440, and *d*400 lattice planes of cubic Y_2O_3, respectively. Additionally, the HRTEM images have also verified that the nanoparticles are free from any apparent lattice defects or dislocations.[31,45]

It has already been shown that Er_2O_3 has the same cubic bixbyite crystal structure as Y_2O_3; the crystal structure has the $Ia3(T_h^7)$ space group with 16 f. u. in the unit cell, possessing 24 yttrium sites having C_2 (noninversion) symmetry and 8 yttrium

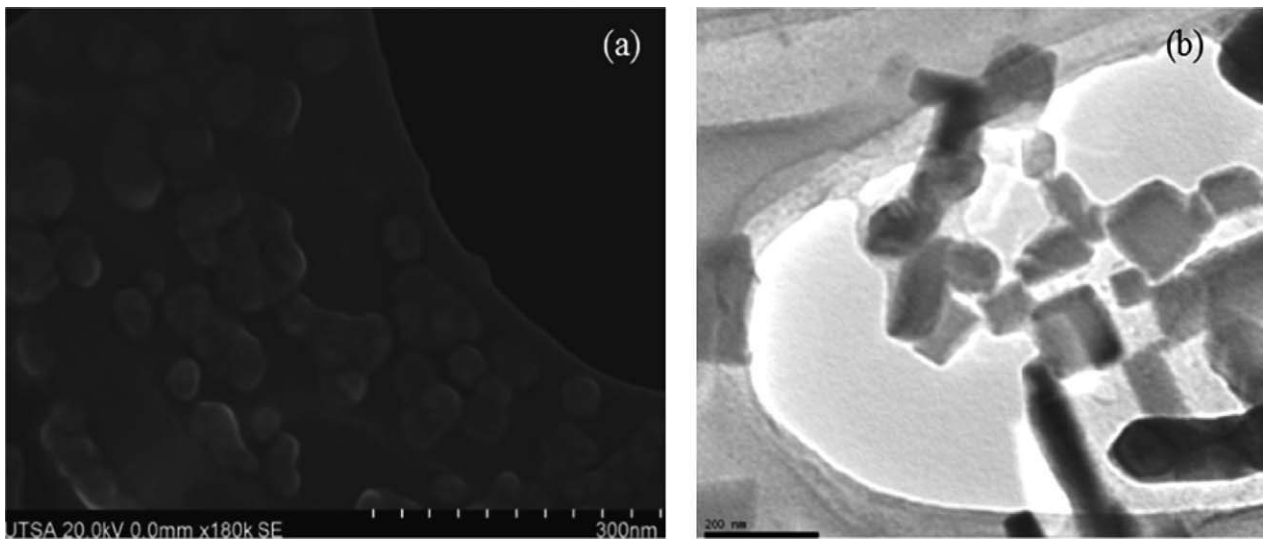

Figure 1 SEM and TEM images of the Er_2O_3 nanoparticles.

sites having C_{3i} (inversion) symmetry.[46–48] The similarities between the emission spectra analysis we reported for the Er^{3+} : Y_2O_3[31] and the experimental and theoretical analyses reported earlier by Kisliuk et al.[23] and Chang et al.,[49] respectively, for Er^{3+} : Y_2O_3 in bulk crystals confirm that our nanoparticles also have the same cubic structure. Er^{3+} ions can substitute into both the C_2 and C_{3i} cation sites.[48,50,51] Even though both electric and magnetic dipole (ED and MD) transitions are reported between the $4I_{15/2}$ and $4I_{13/2}$ manifolds of Er^{3+} in ceramic Er^{3+} : Y_2O_3[25], the inversion symmetry of the C_{3i} site precludes the observation of forced-ED transitions between the Stark levels involving other mutiplet manifolds of Er^{3+}, including those reported in this study. Consequently, all the observed transitions given in Table I can be assigned to the electronic transitions for ions occupying the C_2 sites.

The room-temperature absorption spectrum was taken on the Er_2O_3/PMMA samples using an upgraded Cary model 14R spectrophotometer. The spectrum was taken at 0.1 nm intervals and the spectral bandwidth was automatically maintained at about 0.05 nm for all measurements. The optical transparency of the pure PMMA has already been verified in the 300 to 1600 nm wavelength range.[36] The absorption spectrum taken on the Er_2O_3/PMMA covers the range from 400 to 820 nm and consists of seven $Er^{3+}(4f^{11})$ absorption bands centered around 444, 453, 489, 522, 549, 652, and 804 nm, corresponding to the $^4F_{3/2}$, $^4F_{5/2}$, $^4F_{7/2}$, ^2H $(2)_{11/2}$, $^4S_{3/2}$, $^4F_{9/2}$, and $^4I_{9/2}$ ($^{2S+1}L_J$) multiplet manifolds, respectively. Figure 2 shows the absorption spectrum (in solid black lines) of the Er_2O_3/PMMA sample in the 400 to 850 nm range depicted above the baseline absorption spectrum (in dotted circles) of the PMMA reference sample. The Er_2O_3/PMMA spectrum represents transitions from individual Stark energy levels of the ground-state manifold $^4I_{15/2}$ to the seven upper manifolds mentioned earlier. Transitions are also observed from $Z_2 = 38$, $Z_3 = 75$, $Z_4 = 88$, and $Z_5 = 159$ cm^{-1} excited Stark levels in addition to those from the ground-state Stark level Z_1. These excited Stark level transitions, known as "hot-bands," are characterized by changes in absorption intensity in the excited Stark levels in the spectra recorded at higher temperatures.[35] Spectra obtained by the Cary 14 spectrophotometer at wavelengths shorter than 400 nm and beyond 850 nm are not sufficiently resolved to establish the detailed crystal-field splitting of the multiplet manifolds.

RESULTS AND DISCUSSIONS

Thin discs of trivalent erbium (Er^{3+}) doped erbium oxide (Er_2O_3) nanoparticles suspended in the PMMA matrix were fabricated and studied for the optical properties of Er^{3+} ions in the Er_2O_3/PMMA medium. The nanoparticles used for this purpose were synthesized using a hydrothermal precipitation method. They were found to be cubic having an average diameter of 25 nm. SEM, TEM, and HRTEM characterization techniques were used to study the morphology of these nanoparticles. Figure 1 shows the SEM and TEM images of the synthesized Er_2O_3 nanoparticles. The details on synthesis and morphology can be found in Ref. 31 for the Er^{3+} : Y_2O_3 nanoparticles, synthesized using the same methodology and containing 0.3 atm % of Er^{3+} ions. As mentioned earlier, the HRTEM images distinctly showed the presence of *d*222, *d*440, and *d*400 lattice planes characteristic for the cubic Y_2O_3 and Er_2O_3. Additionally, no apparent lattice defects or dislocations were found the HRTEM images of the nanoparticles.

TABLE I
Stark Level Analysis of the Room-Temperature Absorption Spectrum of Er^{3+} in Er_2O_3/PMMA

$^{2S+1}L_J$	λ (nm)	α[a] (cm^{-1})	Label	Transition	E_{exp}[b] (cm^{-1})	Nanocrystalline E_{exp}[c] (cm^{-1})
$^4I_{9/2}$	814.10	0.62	1	$Z_2 \rightarrow W_1$	12,280	12,285
	811.50	0.69	2	$Z_1 \rightarrow W_1$	12,319	12,324
	810.20	0.30	3	$Z_4 \rightarrow W_2$	12,339	12,345
	809.32	0.17	4	$Z_3 \rightarrow W_2$	12,353	12,357
	806.75	0.25	5	$Z_2 \rightarrow W_2$	12,392	12,397
	804.40	2.21	6	$Z_4 \rightarrow W_3$	12,428	12,424
	804.20	2.08	7	$Z_1 \rightarrow W_2$	12,431	12,435
	801.80	0.37	8	$Z_4 \rightarrow W_5$	12,469	
	799.70	1.12	9	$Z_3 \rightarrow W_4$	12,501	12,500
	798.87	0.68	10	$Z_1 \rightarrow W_3$	12,514	12,514
	798.00	0.84	11	$Z_3 \rightarrow W_5$	12,528	12,529
	797.23	0.38	12	$Z_2 \rightarrow W_4$	12,540	12,538
	795.63	0.85	13	$Z_2 \rightarrow W_5$	12,565	12,566
	795.25	1.04	14		12,571	
	794.90	0.83	15	$Z_1 \rightarrow W_4$	12,577	12,576
	793.30	1.81	16	$Z_1 \rightarrow W_5$	12,602	12,605
$^4F_{9/2}$	664.80	1.92	17	$Z_3 \rightarrow V_1$	15,038	15,044
	663.10	1.41	18	$Z_2 \rightarrow V_1$	15,077	15,082
	661.40	5.73	19	$Z_4 \rightarrow V_2$	15,115	15,110
	661.04	3.17	20	$Z_1 \rightarrow V_1$	15,124	15,121
	659.70	4.40	21	$Z_2 \rightarrow V_2$	15,154	15,160
	658.00	4.98	22	$Z_1 \rightarrow V_2$	15,193	15,199
	657.40	1.69	23	$Z_3 \rightarrow V_3$	15,207	
	655.85	4.24	24	$Z_2 \rightarrow V_3$	15,243	15,242
	655.40	3.28	25	$Z_3 \rightarrow V_4$	15,254	15,257
	654.76	4.13	26		15,269	
	654.30	8.34	27	$Z_1 \rightarrow V_3$	15,279	15,280
	653.72	5.44	28	$Z_2 \rightarrow V_4$	15,293	15,294
	652.15	9.04	29	$Z_1 \rightarrow V_4$	15,330	15,333
	651.40	3.31	30	$Z_3 \rightarrow V_5$	15,347	
	649.35	3.07	31	$Z_2 \rightarrow V_5$	15,396	15,399
	647.90	3.99	32		15,430	
	647.65	5.39	33	$Z_1 \rightarrow V_5$	15,436	15,437
	647.35	3.22	34		15,443	
$^4S_{3/2}$	551.03	0.89	35	$Z_4 \rightarrow U_1$	18,143	18,143
	549.70	1.02	36	$Z_2 \rightarrow U_1$	18,187	18,194
	548.46	2.17	37	$Z_1 \rightarrow U_1$	18,228	18,233
	547.14	2.05	38	$Z_2 \rightarrow U_2$	18,272	
	545.93	1.87	39	$Z_1 \rightarrow U_2$	18,312	18,321
$^2H(2)_{11/2}$	529.54	0.54	40	$Z_5 \rightarrow T_1$	18,879	18,880
	527.00	7.93	41	$Z_3 \rightarrow T_2$	18,970	18,967
	526.50	9.23	42	$Z_4 \rightarrow T_3$	18,988	18,984
	526.10	9.23	43	$Z_2 \rightarrow T_2$	19,003	19,006
	525.80	6.94	44	$Z_2 \rightarrow T_2$	19,013	19,006
	525.25	9.78	45	$Z_1 \rightarrow T_1$	19,033	19,038
	524.45	8.11	46	$Z_1 \rightarrow T_3$	19,062	19,073
	523.05	11.54	47	$Z_3 \rightarrow T_4$	19,113	19,110
	522.35	13.38	48	$Z_2 \rightarrow T_4$	19,139	19,149
	521.35	13.38	49	$Z_1 \rightarrow T_4$	19,176	19,168
	520.65	10.56	50	$Z_2 \rightarrow T_6$	19,201	19,203
	520.25	8.95	51	$Z_1 \rightarrow T_5$	19,216	19,207
	519.80	10.25	52	$Z_1 \rightarrow T_6$	19,233	19,243
$^4F_{7/2}$	493.30	2.02	53	$Z_4 \rightarrow S_1$	20,266	20,256
	492.40	1.91	54	$Z_2 \rightarrow S_1$	20,303	20,306
	491.55	3.38	55	$Z_1 \rightarrow S_1$	20,338	20,345
	491.10	2.39	56	$Z_3 \rightarrow S_2$	20,357	20,361
	489.90	3.12	57	$Z_1 \rightarrow S_2$	20,407	20,398
	489.25	4.57	58	$Z_1 \rightarrow S_2$	20,434	20,437
	488.55	3.35	59	$Z_2 \rightarrow S_3$	20,463	20,467
	487.75	2.78	60	$Z_1 \rightarrow S_3$	20,497	20,506
	486.80	1.52	61	$Z_2 \rightarrow S_4$	20,537	20,534
	486.15	0.91	62	$Z_1 \rightarrow S_4$	20,564	20,573

TABLE I. *Continued*

$^{2S+1}L_J$	λ (nm)	α[a] (cm^{-1})	Label	Transition	E_{exp}[b] (cm^{-1})	Nanocrystalline E_{exp}[c] (cm^{-1})
$^4F_{5/2}$	455.85	0.32	63	$Z_4 \rightarrow R_1$	21,931	21,929
	455.55	0.42	64	$Z_3 \rightarrow R_1$	21,945	21,942
	455.10	0.61	65	$Z_2 \rightarrow R_1$	21,967	21,979
	453.80	1.22	66	$Z_3 \rightarrow R_2$	22,030	
	453.35	1.23	67	$Z_1 \rightarrow R_1$	22,052	22,049
	452.65	0.43	68	$Z_1 \rightarrow R_2$	22,086	22,081
	451.35	0.43	69	$Z_2 \rightarrow R_3$	22,150	
	450.76	0.30	70	$Z_1 \rightarrow R_3$	22,179	22,173
$^4F_{3/2}$	447.70	0.07	71	$Z_2 \rightarrow Q_1$	22,330	22,330
	446.35	0.04	72	$Z_1 \rightarrow Q_1$	22,398	
	444.66	0.55	73		22,483	22,494
	443.83	0.67	74	$Z_2 \rightarrow Q_2$	22,525	
	442.69	0.33	75	$Z_1 \rightarrow Q_2$	22,583	
	442.15	0.27	76		22,610	

[a] Absorption coefficient in cm^{-1}.
[b] Experimental energy values in cm^{-1} (this work).
[c] Experimental energy values for nanocrystalline Er^{3+} : Y_2O_3 (Ref. 35).

After verifying the optical transparency of PMMA, the room-temperature absorption spectra for the Er_2O_3/PMMA samples were taken in wavelength range from 400 to 820 nm and shown in Figure 2. Figures 3–5 show the room-temperature absorption spectra of the $^4S_{3/2}$, $^4F_{9/2}$, and $^4I_{9/2}$ manifolds, respectively. The spectra remain sharp and well-defined for the selected wavelength range. The detailed Stark level analyses of the manifold transitions at room-temperature are given in Table I. Column 1 represents the spectroscopic notation of the corresponding $^{2S+1}L_J$ multiplet manifolds. Columns 2 and 3 enlist the nanometer scale wavelengths and the corresponding absorption coefficients in cm^{-1}, respectively, for the Stark transitions identified from the absorption spectra. The individual peaks in the absorption spectra are conveniently labeled using numbers beginning with 1 and are listed in column 4. Column 5 has identified most of the transitions based on a comparative study of the energy values published earlier.[35] The additional structure found at 647.90 and 647.35 nm (given in column 2 of Table I) appear as satellite structure to the relatively intense peak at 647.65 nm from

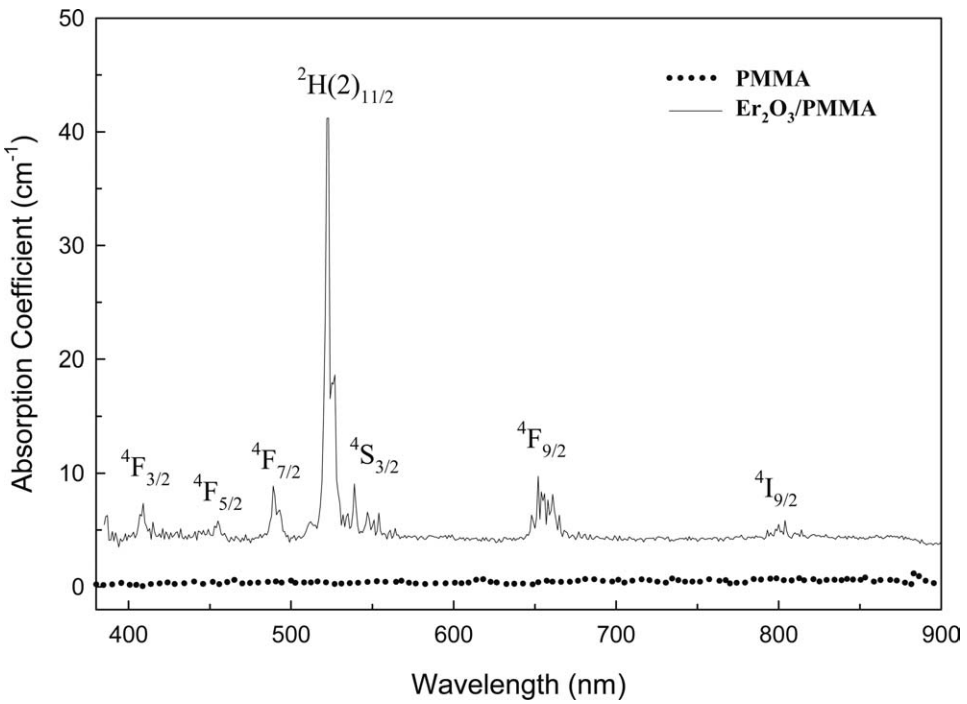

Figure 2 Room-temperature absorption spectrum of PMMA and Er_2O_3/PMMA.

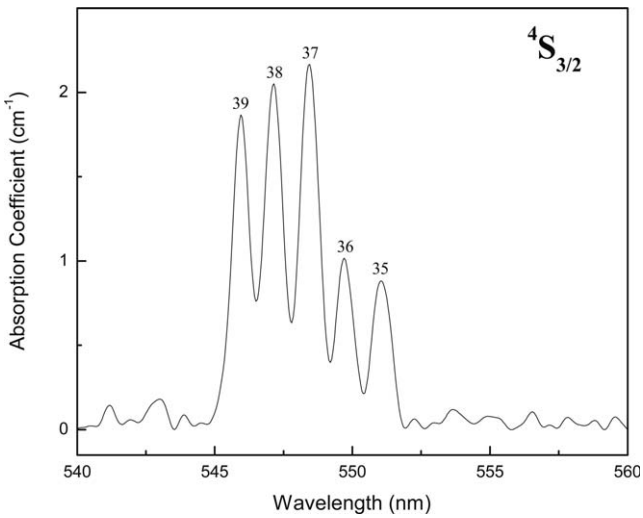

Figure 3 Room-temperature absorption spectrum of the $4S_{3/2}$ manifold for the Er_2O_3/PMMA sample.

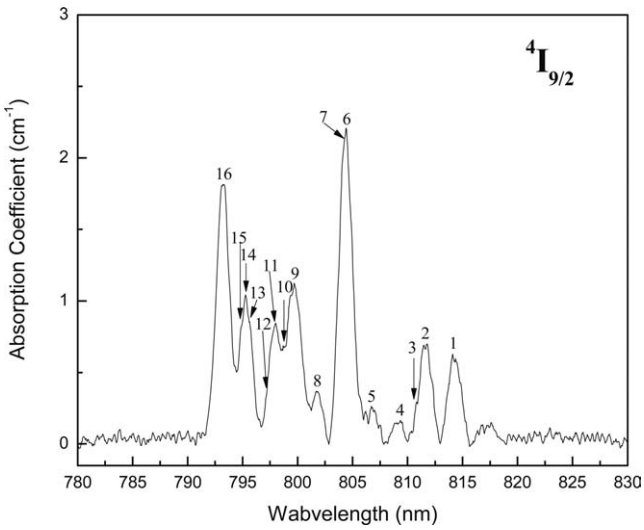

Figure 5 Room-temperature absorption spectrum of the $4I_{9/2}$ manifold for the Er_2O_3/PMMA sample.

$Z_1 \rightarrow V_5$. Also, the 795.25 and 654.76 nm peaks were not assigned. These peaks may be due to a minority site although the origin of all four peaks is unknown at this time. Column 6 gives the experimental energy values in cm^{-1} corresponding to the nanometer wavelength values given in column 2 of Table I. For a comparison analysis, Stark energy levels for the nanocrystalline Er^{3+} : Y_2O_3 sample[35] have been included in column 7 of Table I. As mentioned earlier, the crystal structure is the same for both the cubic Er_2O_3 and Y_2O_3 and in terms of the physical properties, a solid solution exists between them.[46,47]

Our spectroscopic analyses show that the optical properties of the Er_2O_3 nanoparticles embedded in PMMA have many significant similarities with their single-crystal counterparts grown by a flame fusion method.[23,24,49] This reveals that the optical symmetry of Er^{3+} in the nanocrystals is similar to that in the bulk crystalline phase. Additionally, the results show a reasonable agreement between the Stark energy values given in column 6 and 7 of Table I for some selected manifolds of Er^{3+} in the nanocrystalline Er_2O_3/PMMA and Er^{3+} : Y_2O_3[35]samples, respectively. Moreover, in one of our recent publications,[36] it has been verified that the presence of PMMA does not effectively alter the co-ordination environment of the RE^{3+} ions. As mentioned earlier, when suspended in the PMMA matrix, the laser gain-coefficient is found to be increased for the Er^{3+} : Y_2O_3 nanoparticles codoped with Ce^{3+} and Yb^{3+} ions.[6] Studies have also reported the occurrence of energy transfer phenomena from Er^{3+} to other RE^{3+} ions such as Ho^{3+}, Dy^{3+}, and Tm^{3+}. Therefore, our analyses and comparison results can lead to a quantitative study of such interion excitation transfer. In conclusion, the optical transparency of PMMA for a very wide region of optical wavelengths, the sharp absorption peaks obtained at room-temperature for the Er_2O_3/PMMA sample, and the easiness of codoping other RE^{3+} ions into the Er_2O_3/PMMA matrix emphasize that our sample may have future possibilities in various fields such as laser amplifiers and telecommunication devices.

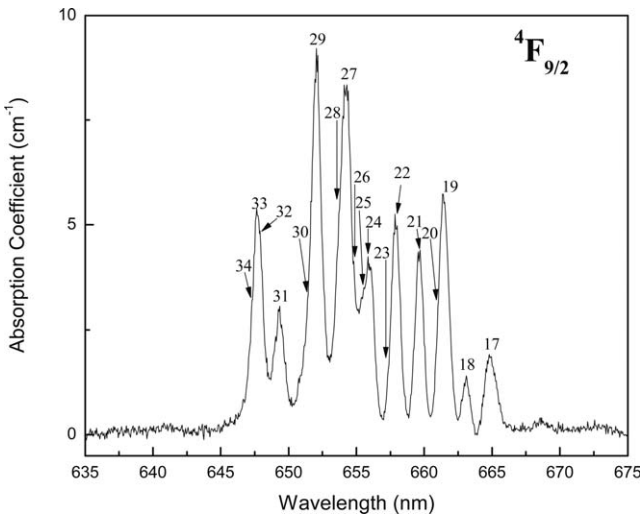

Figure 4 Room-temperature absorption spectrum of the $4F_{9/2}$ manifold for the Er_2O_3/PMMA sample.

CONCLUSIONS

We have described an inexpensive and easier methodology to suspend the nanoparticles of Er_2O_3 in the PMMA matrix. The room-temperature absorption transitions for the sample have been studied in detail for the seven $^{2S+1}L_J$ multiplet manifolds, $^4F_{3/2}$, $^4F_{5/2}$, $^4F_{7/2}$, $^2H(2)_{11/2}$, $^4S_{3/2}$, $^4F_{9/2}$, and $^4I_{9/2}$.The

experimentally obtained Stark energy levels for the above-mentioned manifolds have been analyzed in detail and compare favorably with the results obtained for the nanocrystals of Er^{3+} : Y_2O_3[35]The unique material properties of PMMA and the sharp Stark energy transitions and their excellent agreement with those previously obtained for the Er^{3+} : Y_2O_3 nanocrystal[35] show that the Er_2O_3/PMMA samples described in the present study may serve as an excellent host for many photonic applications. In addition, our results also confirm that the PMMA matrix does not significantly alter the crystal structure or the Er^{3+} symmetry in the Er_2O_3 nanoparticles. Finally, the results obtained from this study indicate that PMMA is an excellent host material for interion energy transfer studies between RE^{3+} ions, and the optical properties investigated here suggest numerous technological applications are possible involving laser systems and fiber-optic telecommunication devices.

The authors acknowledge Dr. Leonard Francis Deepak at the Physics Department and Dr. Waldemar Gorski and Dr. Maogen Zhang at the Chemistry Department of the UTSA for their insightful suggestions on this project.

References

1. Liang, H.; Zheng, Z.; Zhang, Q.; Ming, H.; Chen, B.; Xie, J.; Zhao, H. J Mater Res 2003, 18, 1895.
2. Koeppen, C.; Yamada, S.; Jiang, G.; Garito, A. F.; Dalton, L. R. J Opt Soc Am B 1997, 14, 155.
3. Slooff, L. H.; Dood, M. J. A. D.; van Blaaderen, A.; Polman, A. Appl Phys Lett A 2000, 76, 3682.
4. Kuriki, K.; Koike, Y.; Okamoto, Y. Chem Rev 2002, 102, 2347.
5. Liang, H.; Zheng, Z.; Chen, B.; Zhang, Q.; Ming, H. Mater Chem Phys 2004, 86, 430.
6. Quang, A. Q. L.; Zyss, J.; Ledoux, I.; Truong, V. G.; Jurdyc, A.-M.; Jacquier, B.; Le, D. H.; Gibaud, A. Chem Phys 2005, 318, 33.
7. Donval, A.; Toussaere, E.; Hierle, R.; Zyss, J. J Appl Phys 2000, 87, 3258.
8. Martin, G.; Ducci, S.; Hierle, R.; Josse, D.; Zyss, J.; Appl Phys Lett 2003, 83, 1086.
9. Rittigstein, P.; Priestly, R. D.; Broadbelt, L. J.; Torkelson, J. M. Nat Mater 2007, 6, 278.
10. Peng, L.; Luo, Y.; Dan, Y.; Zhang, L.; Zhang, Q.; Xia, S.; Zhang, X. Colloid Polym Sci 2006, 285, 153.
11. Poort, S. H. M.; Blokpoel, W. P.; Blasse, G. Chem Mater 1995, 7, 1547.
12. Liang, H.; Chen, B.; Zheng, Z. Q. Phys Status Solidi B 2004, 241, 3056.
13. Wong, W. H.; Liu, K. K.; Chan, K. S.; Pun, E. Y. B. J Cryst Growth 2006, 288, 100.
14. Liu, G.; Jacquier, B., Eds. Spectroscopic Properties of Rare Earths in Optical Materials; Springer Series in Materials Science, Springer, Berlin, 2005.
15. Groppi, G.; Cristiani, C.; Forzatti, P. J Mater Sci 1994, 29, 3441.
16. An, L.; Zhang, J.; Liu, M.; Wang, S. J Am Ceram Soc 2005, 88, 1010.
17. Xiao, S.; Yang, X.; Liu, Z.; Yan, X. H. J Appl Phys 2004, 96, 1360.
18. Vetrone, F.; Boyer, J. C.; Capobianco, J. A.; Speghini, A.; Bettinelli, A. J. Appl Phys Lett 2004, 96, 661.
19. Matsuura, D. Appl Phys Lett 2002, 81, 4526.
20. Savio, R. L.; Miritello, M.; Cardile, P.; Priolo, F. J Appl Phys 2009, 106, 043512.
21. Rosenberger, D. Phys Z 1962, 167.
22. Dieke, G. H.; Low, W., Eds. Paramagnetic Resonance; Academic Press: New York, 1963; Vol.1.
23. Kisliuk, P.; Krupke, W. F.; Gruber, J B. J Chem Phys 1964, 40, 3606.
24. Gruber, J. B.; Henderson, J. R.; Muramoto, M.; Rajnak, K.; Conway, J. G. J Chem Phys 1966, 45, 477.
25. Gruber, J. B.; Nash, K. L.; Sardar, D. K.; Valiev, U. V.; Ter-Gabrielyan, N.; Merkle, L. D. J Appl Phys 2008, 104, 023101.
26. Sardar, D. K.; Dee, D. M.; Nash, K. L.; Yow, R. M.; Gruber, J. B. J Appl Phys 2006, 100, 123106.
27. Van, T. T.; Hoang, J.; Ostroumov, R.; Wang, K. L.; Bargar, J. R.; Lu, J.; Blom, H.-O.; Chang, J. P. J Appl Phys 2006, 100, 073512.
28. Dammak, M.; Maalej, R.; Kamoun, M.; Deshchanvres, J.-L. Phys Status Solidi B 2003, 239, 193.
29. Hoang, J.; Van, T. T.; Sawkar-Mathur, M.; Hoex, B.; Van deSanden, C. M.; Kessels, W. M. M.; Ostroumov, R.; Wang, K. L.; Bargar, J. R.; Chang, J. P. J Appl Phys 2007, 101, 1231161.
30. Prasad, P. N., Ed. Nanophotonics; John Wiley & Sons: New York, 2004.
31. Chandra, S.; Deepak, F. L.; Gruber, J. B.; Sardar, D. K. J Phys Chem C 2010, 114, 874.
32. Tanner, P. A.; Wong, K. L. J Phys Chem B 2004, 108, 136.
33. Tanner, P. A.; Zhou, X.; Liu, F. J Phys Chem A 2004, 108, 11521.
34. Sardar, D. K.; Russel, C. C., III; Gruber, J. B.; Allik, T. H. J Appl Phys 2005, 97, 23501.
35. Gruber, J. B.; Sardar, D. K.; Nash, K. L.; Yow, R. M.; Gorski, W.; Zhang, M. J Appl Phys 2007, 101, 113116.
36. Sardar, D. K.; Chandra, S.; Gruber, J. B.; Gorski, W.; Zhang, M.; Shim, J. H. J Appl Phys 2009, 105, 093105.
37. Bian, L.; Qian, X.; Yin, J.; Zhu, Z.; Lu, Q. Mater Sci Eng B 2003, 100, 53.
38. Huang, X.; Brittain, W. J. Macromolecules 2001, 34, 3255.
39. Guo, Y.; Zheng, X.; Ming, H.; Zhang, Q. Chin Phys Lett 2001, 18, 1337.
40. Sun, X.; Liang, H.; Ming, H.; Zhang, Q.; Yang, J.; Zheng, Z.; Ma, H.; Zhang, Y.; Zhang, J.; Xie, J.; Cao, L.; Zhang, Z. Opt Commun 2004, 240, 75.
41. Brenier, A.; Pedrini, C.; Moncorge, R. Opt Quantum Electron 1990, 22, S153.
42. Yu, N.; Liu, F.; Li, X.; Pan, Z. Appl Phys Lett 2009, 95, 231110.
43. Yamauchi, H.; Murigan, G. S.; Ohishi, Y. J Appl Phys 2005, 97, 043505.
44. Hoskins, R. H.; Soffer, B. H. J Quantum Electron 1966, QE-2, 253.
45. Mao, Y.; Huang, J. Y.; Ostroumov, R.; Wang, K. L.; Chang, J. P. J Phys Chem C 2008, 112, 2278.
46. Wyckoff, R. W. G. Crystal Structures; Interscience: New York, 1964; Vol .II.
47. Pauling, L.; Shappell, M. D. Z Krystallogr 1930, 75, 128.
48. Schaack, G.; Koningstein, J. A. J Opt Soc Am 1970, 60, 1110.
49. Chang, N. C.; Gruber, J. B.; Leavitt, R. P.; Morrison, C. A. J Chem Phys 1982, 76, 877.
50. Dean, J. R.; Bloor, D. J Phys C: Solid State Phys 1972, 5, 2921.
51. Gruber, J. B.; Chirico, R. D.; Westrum, E. F. J. J Chem Phys 1982, 76, 4600.